Development and validation of a multiwavelength spatial domain near-infrared oximeter to detect cerebral hypoxia-ischemia

Lindsey A. Nelson
John C. McCann
Andres W. Loepke
Jun Wu
Cincinnati Children's Hospital Medical Center
University of Cincinnati College of Medicine
Department of Anesthesia and Pediatrics
Institute of Pediatric Anesthesia
Cincinnati, Ohio 45229-3039

Baruch Ben Dor
Near Infrared Monitoring Incorporated
Philadelphia, Pennsylvania 19104

C. Dean Kurth
Cincinnati Children's Hospital Medical Center
University of Cincinnati College of Medicine
Department of Anesthesia and Pediatrics
Institute of Pediatric Anesthesia
Cincinnati, Ohio 45229-3039

Abstract. Detection of cerebral hypoxia-ischemia in infants remains problematic, as current monitors in clinical practice are impractical, insensitive, or nonspecific. Our study develops a multiwavelength spatial domain construct for near-infrared spectroscopy (NIRS) to detect cerebral hypoxia-ischemia and evaluates the construct in several models. The NIRS probe contains photodiode detectors 2, 3, and 4 cm from a three-wavelength, light-emitting diode. A construct determines cerebral O_2 saturation based on spatial domain principles. Device performance and construct validity are examined in *in-vitro* models simulating the brain, and in piglets subjected to hypoxia, hypoxia-ischemia, and hyperoxic conditions using a weighted average of arterial and cerebral venous O_2 saturation measured by CO-oximetry. The results in the brain models verify key equations in the construct and demonstrate reliable performance of the device. In piglets, the device measures cerebral O_2 saturation with bias ±4% and precision ±8%. In conclusion, this NIRS device accurately detects cerebral hypoxia-ischemia and is of a design that is practical for clinical application. [DOI: 10.1117/1.2393251]

Keywords: biology; medicine; optical devices; photodetectors; spectroscopy.

Paper 05203RR received Jul. 21, 2005; revised manuscript received Jul. 12, 2006; accepted for publication Jul. 14, 2006; published online Nov. 28, 2006.

1 Introduction

Despite advances in pediatrics over the years, brain damage from hypoxia-ischemia continues to occur.[1,2] Populations at risk of cerebral hypoxia-ischemia include those with congenital heart disease, sickle cell anemia, cerebrovascular disease, and critical illnesses such as prematurity and sepsis. The gold standard to monitor for cerebral hypoxia-ischemia is the neurological examination. However, in these populations, this clinical exam is not reliable because of brain immaturity, systemic illness, or use of sedative drugs. Thus, the diagnosis of cerebral hypoxia-ischemia is often delayed for days to weeks, making it impossible to prevent or treat brain damage.[1,2]

Several technologies exist to monitor the brain, which could be used to detect cerebral hypoxia-ischemia.[3–5] Electroencephalography and cerebral function monitors (CFM) are robust and noninvasive technologies, although they are insensitive or nonspecific for hypoxia-ischemia in the immature, sedated, or anesthetized brain. Jugular bulb oximetry, magnetic resonance imaging, and positron emission tomography are sensitive to cerebral hypoxia-ischemia; however, they are either impractical or unsafe in critically ill infants. Near-infrared spectroscopy (NIRS) is noninvasive and can be applied at the bedside. It uses near-infrared light (700 to 900 nm) to monitor oxygenated and deoxygenated hemoglobin in gas exchanging vessels and can detect cerebral hypoxia-ischemia.[6–12]

Although NIRS holds promise for detecting cerebral hypoxia-ischemia in infants, NIRS has not been used in clinical practice because it has not been able to provide a number that is clinically relevant, accurate, and/or reliable to diagnose cerebral hypoxia-ischemia.[13,14] In the past few years, cerebral O_2 saturation has been identified as a number that is clinically relevant, and methods to verify NIRS accuracy have been established.[6–9,12] Engineering advances should make it possible to improve the reliability and accuracy of NIRS in the clinical environment.[9,13–15] The present study was performed to develop and test a NIRS cerebral oximeter that has hardware features to determine cerebral O_2 saturation in infants.

2 Methods

2.1 *Algorithm*

As with other forms of oximetry, NIRS relies on the Beer-Lambert law, which describes a relationship between light behavior and concentration of a compound:

$$\log(I/I_o) = A + S = (\varepsilon_\lambda LC) + S, \quad (1)$$

where I is the measured power of light at the detector after it passes through the tissue, and I_o is the measured power of

Address all correspondence to: Charles Kurth, Anesthesiology, Cincinnati Children's Hospital, 3333 Burnet Ave, Cincinnati, OH 45246; Tel.: 513-636-7358; Fax: 513-636-7337; E-mail: Dean.Kurth@cchmc.org

1083-3668/2006/11(6)/064022/8/$22.00 © 2006 SPIE

light at the emitter before it enters the tissue. S represents light loss from scattering by the tissue, whereas A represents light loss from absorption by a compound in the tissue. ε_λ is the wavelength-dependent molar absorption coefficient of the absorbing compound, L is the path length of the light from emitter to detector, and C is the concentration of the absorbing compound in the tissue.

For the brain, the light absorbing compounds are mainly oxyhemoglobin (HbO_2) and deoxyhemoglobin (Hb), and to a much lesser extent, water and cytochrome aa_3.[16] If multiple compounds that absorb light are present in the tissue, the total absorbance is the sum of the absorbance by all the absorbing compounds. Thus, Eq. (1) can be transformed to

$$\log(I/I_o) = \varepsilon^{\mathrm{Hb}} L(\mathrm{Hb}) + \varepsilon^{\mathrm{HbO_2}} L(\mathrm{HbO_2}) + A^o + S, \qquad (2)$$

where $\varepsilon^{\mathrm{Hb}}$ and $\varepsilon^{\mathrm{HbO_2}}$ are the molar extinction coefficients of oxy- and deoxyhemoglobin, and A^o is the absorption from other compounds in the tissue (e.g., water, cytochrome aa_3).

S_{O2}, an index of tissue oxygenation, is defined in terms of HbO_2 and Hb and Hb_{total}

$$S_{O2} = \mathrm{HbO_2}/(\mathrm{Hb} + \mathrm{HbO_2}) = \mathrm{HbO_2}/\mathrm{Hb_{total}}, \qquad (3)$$

where Hb_{total} is total hemoglobin concentration per volume of tissue, distinct from blood hemoglobin concentration, which is total hemoglobin concentration per volume of blood. Combining Eqs. (2) and (3) yields

$$\log(I/I_o) = \varepsilon^{\mathrm{Hb}} L(\mathrm{Hb_{total}} - S_{O2}\mathrm{Hb_{total}}) + \varepsilon^{\mathrm{HbO_2}} L(S_{O2}\mathrm{Hb_{total}}) + G, \qquad (4)$$

where G represents A^o and S, as these terms can be considered one and the same with respect to the measure of I by an instrument. Equation (4) contains unknown variables (L, S_{O2}, Hb_{total}, and G), measured variables (I_o and I), and known constants ($\varepsilon^{\mathrm{HbO_2}}$ and $\varepsilon^{\mathrm{Hb}}$). It is possible to solve for S_{O2} through a multiequation technique in which equations are constructed using the domains of wavelength, time, frequency, or space. Our approach combines the wavelength and spatial domains.

In the wavelength domain, the emitter and detector distance is held constant and the wavelengths are allowed to vary. For a given wavelength pair at a given emitter and detector distance, assuming constancy of G between the wavelengths, Eq. (4) can be simplified to

$$R = aL\mathrm{Hb_{total}} + bL\mathrm{Hb_{total}}S_{O2}, \qquad (5)$$

where a and b are lump constants for the molar extinction coefficients of Hb and HbO_2 at the two wavelengths, and R is the ratio of the measured intensities at the two wavelengths. Of note, Eq. (5) represents a linear function between R and S_{O2} for any given wavelength pair and emitter-detector distance.

In the spatial domain, the wavelength is held constant and the emitter and detector distance is allowed to vary. Path length and emitter-detector distance (D) are related through a constant known as the differential path length factor (F)

$$L = DF. \qquad (6)$$

For a given detector pair measuring light intensity from a single emitter, assuming constancy of Hb and HbO_2 in the optical field, Eq. (2) can be developed to yield

$$r = L_1(\varepsilon^{\mathrm{Hb}}\mathrm{Hb} + \varepsilon^{\mathrm{HbO_2}}\mathrm{HbO_2}) - L_2(\varepsilon^{\mathrm{Hb}}\mathrm{Hb} + \varepsilon^{\mathrm{HbO_2}}\mathrm{HbO_2}), \qquad (7)$$

where r is the ratio of the measured intensities at the two detectors and L_1 and L_2 are optical path lengths. If the wavelength at which I is measured such that $\varepsilon^{\mathrm{Hb}}$ and $\varepsilon^{\mathrm{HbO_2}}$ are equal (isobestic point), then Eq. (7) can be simplified to

$$r = \varepsilon^{\mathrm{Hb}}\mathrm{Hb_{total}}(L_1 - L_2). \qquad (8)$$

Combining Eqs. (6) and (8) yields

$$\mathrm{Hb_{total}} = r/(\varepsilon^{\mathrm{Hb}} F \Delta D), \qquad (9)$$

where ΔD represents the distance between the detector pair. Of note, a linear relationship exists between r and Hb_{total}.

Combining the wavelength and spatial domains expressed by Eqs. (5) and (9) and then simplifying gives

$$R = rAD/\Delta D + rBD/\Delta D S_{O2}, \qquad (10)$$

in which A and B denote lump constants for the extinction coefficients of Hb and HbO_2. Using Eq. (10), it is possible to construct an algorithm to determine S_{O2} by measuring light intensities at two or more detectors separated by different distances from a light source emitting at two or more wavelengths, in which one wavelength is at the isobestic point.

Boundary conditions around the emitter and detector can also affect optical pathlength and light intensity to create error or noise in the measurement of S_{O2} from D, R, and r.[17,18] Several methods exist to control this effect, including the use of light shields around the emitter, detector, and tissue; the use of materials and designs to improve coupling between the emitter, detector, and tissue; and the application of robust algorithms and signal processing. In our experience, no single method has been satisfactory. Thus, our approach relies on the design of an optical probe housing the emitter and detector to enhance light shielding and light-tissue coupling, as well as algorithm and signal processes to reduce aberrant signals.

For the algorithm, S_{O2} is determined from the average of several wavelength pairs and emitter-detector distances. If Eq. (10) is solved for S_{O2}, in which the detector pair to determine r is 1 cm apart ($\Delta D = 1$), then

$$S_{O2} = (R - rAD)/(rBD). \qquad (11)$$

Expanding Eq. (11) to include several wavelength pairs and emitter-detector distances yields an expression

$$S_{O2} = \left[\sum_{i=1}^{N_\lambda} \sum_{j=1}^{N_\delta} (R_{i,j} - r_j A_i D_j)/(r_j B_i D_j) \right] / N_\lambda N_\delta, \qquad (12)$$

where N_λ is the number of wavelength pairs and N_δ is the number of emitter-detector distances.

2.2 *Materials*

A prototype NIRS device was constructed (Near Infrared Monitoring Incorporated, Philadelphia, Pennsylvania). It consisted of a probe housing light emitters and three photodiode detectors separated from the emitter by 2, 3, and 4 cm. The emitter contained light emitting diodes at 730, 805, and 850 nm. The 805-nm wavelength is an isobestic point for oxy- and deoxyhemoglobin. The emitter and detectors were housed within a soft plastic shell, connected to the main unit by a wire bundle. The emitter and detectors were recessed within the probe to provide light shielding, while the material for the probe was lightweight and highly compliant to facilitate probe-tissue coupling. The main unit contained the electronic hardware to capture the signals at each wavelength and detector. After power-up, the device undergoes an internal calibration to check the integrity of the hardware. Application of this device to Eq. (12) results in the measurement of nine values for R and one value for r, each captured at 3 Hz and signal averaged over 10 s.

An *in-vitro* "static" brain model consisting of India ink and intralipid admixed in a gelatin polymer to mimic the optical density of the human head was used to determine instrument signal-to-noise and drift. An *in-vitro* "dynamic" brain model simulating the brain was used to test Eqs. (5) and (9) and to develop the algorithm per Eq. (12).[19] This model contained a microvascular network perfused with human blood in which S_{O2} and Hb_{total} could be varied. Blood S_{O2} was measured by CO-oximetry (OSM™ 3, Hemoximeter™, Radiometer Copenhagen, Copenhagen NV, Denmark). Blood gas analysis was performed (iSTAT, iSTAT Corporation, Princeton, New Jersey). pH and PCO_2 were maintained at 7.35 to 7.45 and 35 to 45 torr, respectively.

A piglet model was used to test the algorithm [Eq. (12)] prospectively. After approval by the Institutional Animal Care and Use Committee, 13 piglets aged 4 to 6 days were studied. Anesthesia was induced with intramuscular ketamine (33 mg/kg) and acepromazine (3.3 mg/kg), and maintained with fentanyl (25 μg/kg bolus, then 10 μg/kg/h) and midazolam (0.2 mg/kg bolus, then 0.1 mg/kg/h). Following tracheal intubation and mechanical ventilation, catheters were inserted into the femoral artery and superior sagittal sinus to sample blood for arterial saturation (Sa_{O2}) and cerebral venous saturation (Ss_{O2}). In six piglets, an incision was made in the neck, the carotid arteries were isolated, and ligatures were placed around the vessels to produce cerebral ischemia.

2.3 *Protocols*

In the static model, 3 h of NIRS data were recorded to determine static signal-to-noise and signal drift. To determine the effect of probe positioning on signal-to-noise (dynamic signal-to-noise), the probe was repositioned 15 times in the same location. NIRS data were recorded before and after each positioning. In the dynamic model, Eq. (5) was examined by increasing SO_2 from 0 to 100%, and blood samples from the model and NIRS data were recorded at each increment. Experiments were performed at two different blood Hb_{total}. To test Eq. (9), Hb_{total} was decreased from 15 to 5 g/dl in 2 g/dl steps, while S_{O2} was held at 70%. Blood samples from the model and NIRS data were recorded at each hemoglobin concentration.

In the piglet experiments, inspired O_2 (FiO_2), minute ventilation, and cerebral perfusion were varied to force cerebral O_2 saturation over a wide range during high and low cerebral blood volume conditions. Piglets were divided into a hypoxia group and a hypoxia-ischemia group, in which the hypoxia-ischemia group had both carotid arteries completely occluded during the hypoxia conditions. The following conditions were produced. 1. Normoxia: room air was inspired with minute ventilation adjusted to normocapnia. 2. Hypercapnia/hyperoxia: FiO_2 was 100% and minute ventilation was decreased to a 10% expired CO_2. 3. Mild hypoxia: FiO_2 was decreased to 17%. 4. Moderate hypoxia: FiO_2 was decreased to 13%. 5. Severe hypoxia: FiO_2 was decreased to 8%. After 5 min at each condition, NIRS SO_2 (Sc_{O2}), arterial pressure, arterial blood gases, and pH, Sa_{O2} and Ss_{O2} were recorded. After the experiment, piglets were euthanized with intravenous pentobarbital 100 mg/kg.

2.4 *Data Analysis*

Data are presented as mean ±SD. For the static model, drift was

$$\text{drift} = 100^{*}[(\text{initial } Sc_{O2} - \text{end } Sc_{O2})/\text{initial } Sc_{O2}]/3 \text{ h}, \tag{13}$$

where the initial and end Sc_{O2} represent the average Sc_{O2} over five minutes at the beginning and end of the 3-h experiment. Instrument static signal-to-noise and dynamic signal-to-noise were

$$\text{signal-to-noise} = 100^{*}(\text{SD of } Sc_{O2})/(\text{average } Sc_{O2}), \tag{14}$$

where the average Sc_{O2} is the average value over 3 h for the static signal-to-noise, and the average of the 15 values from positioning for the dynamic signal-to-noise.

For the dynamic model, linearity of R and S_{O2} [Eq. (5)], and r and Hb_{total} [Eq. (9)], were determined by least squares regression. For the piglet model, blood S_{O2} in the cerebrovasculature may be approximated by Sm_{O2}, a weighted average of Sa_{O2} and Ss_{O2}[7,8,13,19]

$$Sm_{O2} = 0.85(Sa_{O2}) + 0.15(Ss_{O2}). \tag{15}$$

Algorithm accuracy for Sc_{O2} was evaluated in terms of Sm_{O2} by least squared regression, as well as by the bias and precision.[20,21] Unpaired T-tests with bonferroni correction were used to compare Sc_{O2}, Sa_{O2}, and Ss_{O2} between conditions.

3 Results

Table 1 displays NIRS device performance in the static brain model. Drift varied from 2%/h to −2%/h among the ratios and detectors, the average being <1%. Static signal-to-noise ranged from 0.1 to 1.9% among the ratios and detectors, the average being <1%. The dynamic signal-to-noise ranged from 12 to −9% among the ratios and detectors, the average being 2.6%. The dynamic signal-to-noise was significantly less at the 4-cm emitter-detector than at the 2- and 3-cm

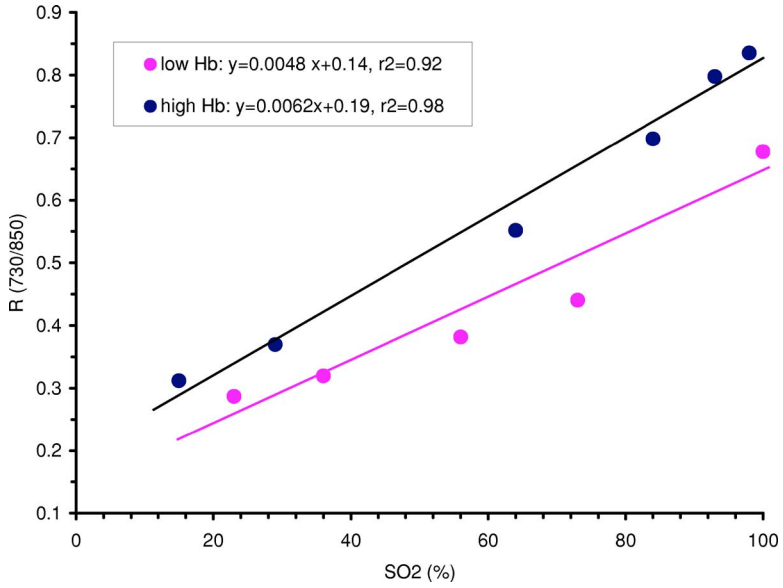

Fig. 1 Response of the wavelength pair intensity ratio (R) for 730 and 850 nm measured at the 4-cm detector by the NIRS oximeter, to O_2 saturation (S_{O2}) of blood perfusing the brain model. There was a highly linear response, although hemoglobin concentration of the blood significantly altered it.

emitter-detectors ($p<0.001$). The dynamic signal-to-noise was significantly greater than the static signal-to-noise at each emitter-detector pair ($p<0.001$).

Table 2 and Figs. 1 and 2 illustrate the dynamic brain model experiments. Linear relationships with excellent correlations were observed between S_{O2} and the intensity ratios for all wavelength pairs (R) at all detectors (Table 2), verifying the relationship in Eq. (5). Slopes and intercepts increased significantly as emitter-detector distance increased (all $p<0.01$), in keeping with the effect of the longer path length at the greater emitter-detector distances in Eqs. (5) and (6). Although linear relationships were observed at each hemoglobin concentration (Fig. 1), the slopes and intercepts were significantly greater at the higher hemoglobin concentration compared with those at the lower hemoglobin concentration, as predicted in Eq. (5). In Fig. 2, a linear relationship was observed between hemoglobin concentration and intensity ratios for a distance pair at 805 nm (r), as predicted from Eq. (9).

Tables 3 and 4 list the blood gases and pH, as well as Sa_{O2}, Ss_{O2}, and NIRS Sc_{O2} in the test piglet experiments. Arterial blood values were not significantly different between the hypoxia and hypoxia-ischemia groups, except at 17 and 9% FiO_2, where Ss_{O2} in the hypoxia group was significantly greater than in the hypoxia-ischemia group.

Figures 3 and 4 display the device algorithm performance during the test piglet experiments. There were linear relationships with excellent correlations between the NIRS Sc_{O2} and Sm_{O2} (Fig. 3, $y=0.96-5$, $r^2=0.92$) and Ss_{O2} ($y=0.87-13$, $r^2=0.89$). The bias and precision, respectively, for the NIRS Sc_{O2} was −4 and 8% relative to Sm_{O2} (Fig. 4), and −9 and 10% relative to Ss_{O2}. Bias, precision, and correlation were similar in the hypoxia and hypoxia-ischemia groups.

4 Discussion

Hypoxia-ischemic brain injury continues to occur in certain pediatric populations.[1,2] The present study developed a NIRS

Table 1 NIRS cerebral oximeter performance in a static brain model. A, B, and C represent wavelength intensity ratios for 730/850 nm, 730/805 nm, and 850/805 nm, respectively. s/n is signal to noise. E-D is the distance between emitter and detector. % represents the actual ΔSc_{O2} from drift or signal-to-noise (see Eqs. (13) and (14) in Sec. 2).

E-D (cm)	2			3			4			
	A	B	C	A	B	C	A	B	C	Mean
Drift (%/h)	−1.0	−1.2	2.1	−1.8	−1.7	−0.2	−0.9	−1.4	0.3	−0.6
Static s/n (%)	0.1	0.3	1.1	0.3	0.2	1.9	0.2	0.3	0.2	0.6
Dynamic s/n (%)	12	8.0	9.0	9.0	9.0	−9.0	1.0	1.0	−1.0	2.6

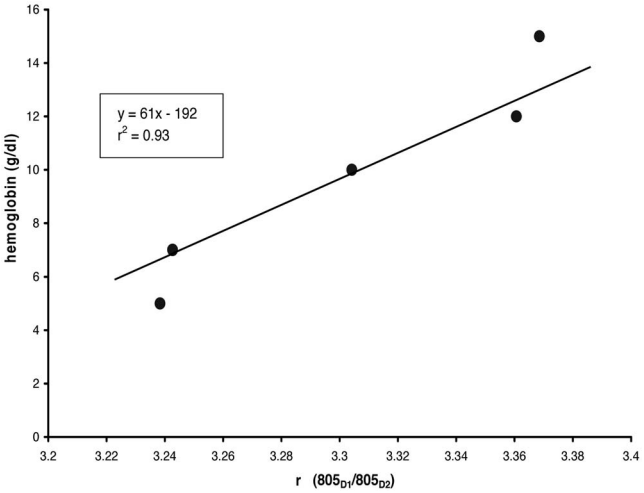

Fig. 2 Response of the detector pair intensity ratio (*r*) for 1- and 2-cm detectors measured at 805 nm by the NIRS oximeter, to hemoglobin concentration of blood perfusing the brain model. There was a highly linear response.

spatial domain construct to detect cerebral hypoxia-ischemia, built a device to use the construct, evaluated the device and construct in several brain models, and tested the construct-algorithm to measure cerebral O_2 saturation in a piglet hypoxia-ischemia model. The results demonstrated reliable performance of the device in brain models, verified key equations in the construct in the brain models, and observed accurate measurement of cerebral O_2 saturation with respect to the surrogate measures of Sm_{O2} and Ss_{O2} in the animal model.

Over the years, several issues have hampered the use of NIRS in clinical practice. These issues relate to the measure of tissue oxygenation, experimental methods to validate this measure, the availability of clinically practical devices, and identification of critical tissue oxygenation values to guide diagnosis and therapy.[13–15,20] In brain tissue, the oxygen-sensitive compounds that absorb near-infrared light include hemoglobin and cytochrome aa_3.[16] It is therefore possible to apply NIRS to measure hemoglobin oxygenation and/or cytochrome aa_3 oxygenation, reflecting an assessment of the intravascular and the intracellular compartments, respectively. In theory, it is preferable to know intracellular oxygenation, because that is where oxidative metabolism occurs and insufficient oxidative metabolism ultimately leads to energy failure and cell death. Moreover, although tight coupling exists between intravascular and intracellular oxygenation, uncoupling can occur in rare situations (e.g., carbon monoxide poisoning, brain death).[10–12] However, at the present time, cytochrome aa_3 measurement is technically difficult and prone to error in the clinical environment.[22–24] Thus, a practical approach to detect cerebral hypoxia-ischemia in these rare situations is to measure hemoglobin oxygenation with neurophysiological function (eg., EEG).[23]

NIRS hemoglobin oxygenation has been measured in terms of oxyhemoglobin concentration (Hb_{O_2}), oxy-deoxy hemoglobin concentration difference (Hb_{diff}), O_2 saturation (Sc_{O2} or rS_{O2}), and tissue oxygenation index (Ti_{O_2}).[6–9,11,25] Because HbO_2 and Hb_{diff} are mass per volume of tissue measurements, they indicate tissue oxygenation. Because O_2 flux from blood to the mitochondria is driven by O_2 partial pressure linked to the oxy-hemoglobin dissociation curve, Sc_{O2}, rS_{O2}, and Ti_{O_2} indicate tissue oxygenation. For historical reasons, clinicians use O_2 saturation to describe blood oxygenation. We selected O_2 saturation as the term to describe cerebral oxygenation, because it is a clinically user-friendly term and other instruments exist to measure it (e.g., CO-oximetry), which helps with validation.

Experimental methods to validate NIRS have been problematic.[13,20] Validation requires a comparison of the measurements made by the new device against a standard; the accuracy of the new device is then expressed in terms of bias and precision relative to the standard.[20,21] NIRS monitors a mixed vascular bed dominated by gas-exchanging vessels, especially venules.[8,26] Because no other device measures such a mixed vascular oxygenation, NIRS has lacked a standard to validate it. However, in situations where no standard exists, it is still possible to validate a device using a surrogate, or the average of two or more surrogates, which approximates the standard.[21] In our study, we used Sm_{O2}, a weighted average of Sa_{O2} and Ss_{O2}, as the main surrogate, and Ss_{O2} alone as a minor surrogate. Not surprisingly, we observed that the bias and precision was higher against Ss_{O2}, because it introduces error from the omission of the arterial contribution viewed by NIRS. Although Sm_{O2} contains an arterial contribution and is better than Ss_{O2}, it introduces error because it uses a constant venous: arterial ratio, which has been shown to vary slightly among subjects and conditions.[8] Thus, some imperfection in

Table 2 NIRS oximeter performance in a dynamic brain model. Abbreviations same as Table 1. Slope, intercept, and r^2 are for the line between the wavelength pair intensity ratio [*R* in Eq. (12) in Sec. 2] calculated by the device and O_2 saturation (SO_2) of blood perfusing the brain model.

E-D (cm)	2			3			4		
	A	B	C	A	B	C	A	B	C
Ratio versus S_{O2}									
Slope	38	31	−18	51	40	−24	62	51	−33
intercept	37	47	121	35	46	122	19	29	129
r^2	0.99	0.99	0.99	0.98	0.99	0.99	0.98	0.98	0.98

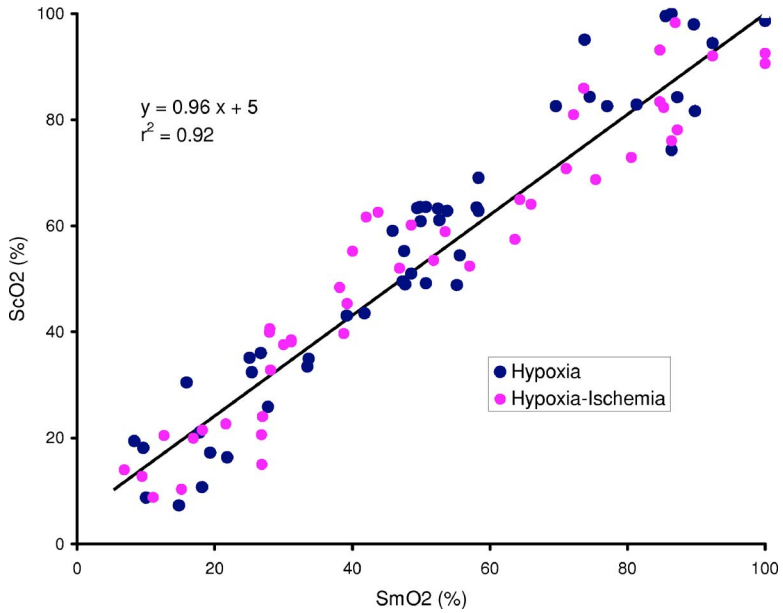

Fig. 3 NIRS oximeter performance in piglets subjected to hypoxia (n=6) or hypoxia-ischemia (n=7). Sc_{O2} is cerebral O_2 saturation measured by the NIRS oximeter, and Sm_{O2} is the weighted average cerebral O_2 saturation [Eq. (15)] measured by CO-oximetry. Line indicates regression. There is a highly linear relationship.

the bias, precision, and correlation originates from the Sm_{O2} surrogate. It might be possible to assess the imperfection by estimating the arterial contribution in the Sm_{O2} of each piglet through the measurement of the pulsatile (arterial) component of the optical signal.

How accurate does NIRS have to be for clinical application? There are no clinical studies to answer this, although animal data suggest a precision of 10% is needed. Cerebral O_2 saturation in healthy humans and piglets is 55 to 75%.[8,12,13] In piglets, after cerebral O_2 saturation decreases to 40%, brain function becomes disturbed.[12,13] Thus, the cushion between normal and dysfunctional in piglets is 15% at a minimum, at the precision of the device (±8%). Thus, the accuracy of the device appears sufficient to warrant clinical trials to determine application in pediatrics.

To determine O_2 saturation, it is necessary to account for the effects of light scattering and optical path length.[17] Time domain, frequency domain, or spatial domain principles were developed for this purpose. We used the spatial domain because of advantages in engineering and costs over time- and frequency-domain technologies. The spatial domain requires equality of light scattering among the wavelengths and equality of O_2 saturation in the optical fields among the emitter-detectors [see Eqs. (5) and (8)]. The results indicate that these assumptions were reasonably met for the models employed in our study.

The limitation of spatial domain relates to the different optical paths among the emitter-detector combinations. Computer simulations have shown three possible routes for photons to take after leaving the emitter.[17,27] 1. shallow—these photons deflect off the scalp, skull, or neocortical surface and

Table 3 Physiological parameters in the piglet hypoxia-ischemia model. Values are mean ± SD, n=13. PCO_2, PO_2, and MAP represent arterial partial pressure of carbon dioxide and oxygen, and mean arterial pressure, respectively.

Condition	pH	PCO_2 (torr)	PO_2 (torr)	MAP (mmHg)
Normoxia	7.47±0.06	36±4	77±8	86±13
Hypercapnic-hyperoxia	7.13±0.05	90±14	401±84	83±13
Hypoxia 17%	7.52±0.09	33±3	59±9	83±9
Hypoxia 13%	7.49±0.08	34±3	36±10	80±12
Hypoxia 9%	7.48±0.01	35±3	22±4	68±13

Table 4 Arterial, cerebral venous sinus, and NIRS cerebral O_2 saturation in the piglet model. Values are mean±SD. N=7 for H and n=6 for HI. H is hypoxia only; H-I is hypoxia and ischemia. $^*p$ <0.01 H versus HI. Sa_{O2}, Ss_{O2}, and Sc_{O2} are arterial, sagittal sinus (cerebral venous), and NIRS cerebral O_2 saturation, respectively.

Condition	Sa_{O2} (%)		Ss_{O2} (%)		Sc_{O2} (%)	
	H	H-I	H	H-I	H	H-I
Normoxia	96±1	96±3	40±3	44±9	55±7	54±5
Hypercapnic-hyperoxia	99±3	100±0	88±6	87±7	93±10	89±8
Hypoxia 17%	93±4	90±4	35±11	19±6*	46±10	38±8
Hypoxia 13%	75±15	64±13	23±15	14±3	25±9	24±6
Hypoxia 9%	46±15	36±14	14±5	6±1*	17±9	12±2

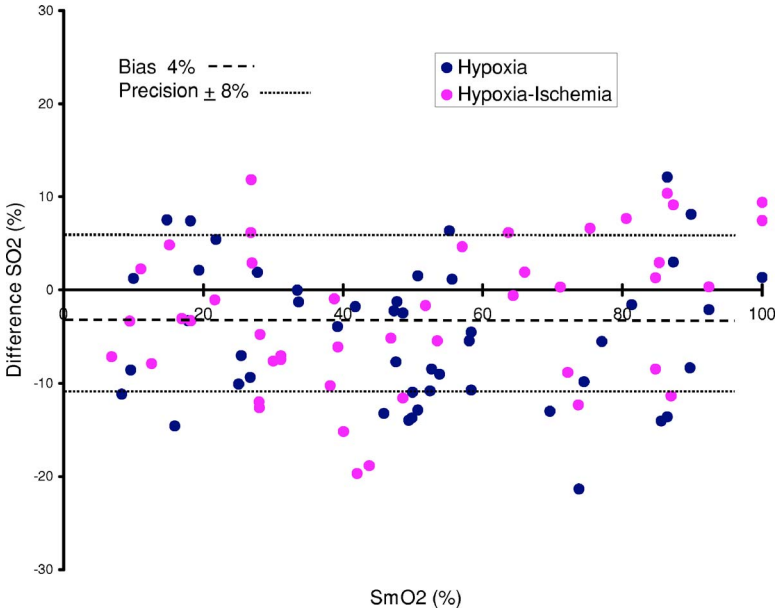

Fig. 4 NIRS oximeter performance in the same piglets as Fig. 3. Difference S_{O2} is the difference between Sc_{O2} and Sm_{O2}. Dashed and dotted lines indicate bias and precision.

never make it to the detectors; 2. deep—these photons scatter indefinitely and never exit from the head; 3. middle—these photons encounter multiple scattering events before making their way to the detectors. The middle photons appear to travel within a banana-shaped field, the depth of which approximates one third the emitter-detector distance.[18,27] Our optical probe contained emitter-detector distances of 2, 3, and 4 cm, which would give penetration depths of approximately 0.6, 1, and 1.3 cm, corresponding to the "bananas" being in the neocortex and basal ganglia.

Considering the various optical paths, the following errors might occur with our device. First, it would not detect focal ischemia outside the optical field. For instance, a probe located on the forehead and monitoring the frontal neocortex would not detect ischemia in the occipital neocortex. Second, it would not detect highly focal ischemia within an optical field that was otherwise well oxygenated. For example, the probe would not detect laminar ischemia in white matter while the overlying gray matter was normally oxygenated. Thus, the spatial-domain device is best suited to detect global cerebral hypoxia-ischemia, as in our piglet model.

Motion artifact, drift, and other noise hinder NIRS devices from being practical, reliable, and accurate in the clinical environment. In our study, the drift and static signal-to-noise were small in comparison to the dynamic signal-to-noise, which at the individual detectors was up to Sc_{O2} 12% and of a magnitude that could be troublesome in the clinical environment, as the buffer between normal and dysfunctional is approximately Sc_{O2} 15%.[8,12,13] Boundary conditions around the emitter and detector create this error by affecting D, R, and r in Eq. (10).[17,18] We employed the use of multiple-wavelength ratios in the algorithm, longer emitter-detector distances (see Table 1), and a lightweight optical probe to facilitate optical-tissue coupling. Nevertheless, other solutions will be required to lessen this noise.

NIRS devices have employed time-, frequency-, and spatial-domain principles to determine cerebral oxygen saturation.[7–9,12,15,18,22,28] In laboratory settings, studies of frequency- and time-domain devices report accuracy similar to our study.[9,15,28] Studies of commercially available spatial-domain devices reveal poor agreement among the devices and less accuracy compared with our study.[7,18,29]

In summary, our prototype NIRS device uses inexpensive, robust, and clinically friendly technology similar to pulse oximetry. The device uses a multiwavelength spatial domain construct and is sufficiently accurate to diagnose cerebral hypoxia-ischemia in piglets. Before clinical use, human studies to validate the device and optical probe design work are indicated.

Acknowledgments

The authors wish to thank Melinda Chappell for editorial assistance. This work was supported by National Institutes of Health grant R42 NS039707.

References

1. D. M. Ferriero, "Neonatal brain injury," *N. Engl. J. Med.* **351**, 1985–1995 (2004).
2. R. C. Vannucci and J. M. Perlman, "Interventions for perinatal hypoxic-ischemic encephalopathy," *Pediatrics* **100**, 1004–1014 (1997).
3. H. L. Edmonds, Jr., Y. P. Zhang, and C. B. Shields, "New neurophysiology and central nervous system dysfunction," *Curr. Opin. Crit. Care* **9**, 98–105 (2003).
4. K. A. Hossmann, "Viability thresholds and the penumbra of focal ischemia," *Ann. Neurol.* **36**, 557–565 (1994).
5. W. D. Heiss, "Ischemic penumbra: evidence from functional imaging in man," *J. Cereb. Blood Flow Metab.* **20**, 1276–1293 (2000).
6. N. C. Brun, A. Moen, K. Borch, O. D. Saugstad, and G. Greisen, "Near-infrared monitoring of cerebral tissue oxygen saturation and blood volume in newborn piglets," *Am. J. Physiol.* **273**, H682–H686 (1997).

7. P. E. F. Daubeney, S. N. Pilkington, E. Janke, G. A. Charlton, D. C. Smith, and S. A. Webber, "Cerebral oxygenation measured by near-infrared spectroscopy: comparison with jugular bulb oximetry," *Ann. Thorac. Surg.* **61**, 930–934 (1996).
8. H. M. Watzman, C. D. Kurth, L. M. Montenegro, J. Rome, J. M. Steven, and S. C. Nicolson, "Arterial and venous contributions to near-infrared cerebral oximetry," *Anesthesiology* **93**, 947–953 (2000).
9. S. Fantini, D. Hueber, M. A. Franceschini, E. Gratton, W. Rosenfeld, P. G. Stubblefield, D. Maulik, and M. R. Stankovic, "Non-invasive optical monitoring of the newborn piglet brain using continuous-wave and frequency-domain spectroscopy," *Phys. Med. Biol.* **44**, 1543–1546 (1999).
10. S. Nioka, B. Chance, D. S. Smith, A. Mayevsky, M. P. Reilly, C. Alter, and T. Asakura, "Cerebral energy metabolism and oxygen state during hypoxia in neonate and adult dogs," *Pediatr. Res.* **28**, 54–62 (1990).
11. R. Springett, J. Newman, M. Cope, and D. T. Delpy, "Oxygen dependency and precision of cytochrome oxidase signal from full spectral NIRS of the piglet brain," *Am. J. Physiol. Heart Circ. Physiol.* **279**, H2202–H2209 (2000).
12. C. D. Kurth, W. J. Levy, and J. Mccann, "Near-infrared spectroscopy cerebral oxygen saturation thresholds for hypoxia-ischemia in piglets," *J. Cereb. Blood Flow Metab.* **22**, 335–341 (2002).
13. S. K. Samra, E. A. Dy, K. Welch, P. Dorje, G. B. Zelenock, and J. C. Stanley, "Evaluation of a cerebral oximeter as a monitor of cerebral ischemia during carotid endarterectomy," *Anesthesiology* **93**, 964–970 (2000).
14. T. Mille, M. E. Tachimiri, C. Klersy, G. Ticozzelli, G. Bellinzona, I. Blangetti, S. Pirrelli, M. Lovotti, and A. Odero, "Near infrared spectroscopy monitoring during carotid endarterectomy: which threshold value is critical?," *Eur. J. Vasc. Endovasc Surg.* **27**, 646–650 (2004).
15. C. D. Kurth and W. S. Thayer, "A multiwavelength frequency-domain near-infrared cerebral oximeter," *Phys. Med. Biol.* **44**, 727–740 (1999).
16. S. Wray, M. Cope, D. T. Delpy, J. S. Wyatt, and E. O. Reynolds, "Characterization of the near infrared absorption spectra of cytochrome aa3 and haemoglobin for the non-invasive monitoring of cerebral oxygenation," *Biochim. Biophys. Acta* **933**, 184–192 (1988).
17. E. M. Sevick, B. Chance, J. Leigh, S. Nioka, and M. Maris, "Quantitation of time- and frequency-resolved optical spectra for the determination of tissue oxygenation," *Anal. Biochem.* **195**, 330–351 (1991).
18. S. Arridge and D. T. Delpy, "The theoretical basis for the determination of optical pathlengths in tissue: temporal and frequency analysis," *Phys. Med. Biol.* **37**, 1531–1560 (1992).
19. C. D. Kurth, H. Liu, W. S. Thayer, and B. Chance, "A dynamic phantom brain model for near-infrared spectroscopy," *Phys. Med. Biol.* **40**, 2079–2092 (1995).
20. V. Pollard, D. S. Prough, E. DeMelo, D. J. Deyo, T. Uchida, and H. F. Stoddart, "Validation in volunteers of a near-infrared spectroscope for monitoring brain oxygenation in vivo," *Anesth. Analg. (Baltimore)* **82**, 269–277 (1996).
21. J. M. Bland and D. G. Altman, "Statistical methods for assessing agreement between two methods of clinical measurement," *Lancet* **1986**, 307–310.
22. M. Ferrari, L. Mottola, and V. Quaresima, "Principles, techniques, and limitations of near infrared spectroscopy," *Can. J. Appl. Physiol.* **29**, 463–487 (2004).
23. T. Sakamoto, R. A. Jonas, U. A. Stock, S. Hatsuoka, M. Cope, R. J. Springett, and G. Nollert, "Utility and limitations of near-infrared spectroscopy during cardiopulmonary bypass in a piglet model," *Pediatr. Res.* **49**, 770–776 (2001).
24. K. Uludag, M. Kohl, J. Steinbrink, H. Obrig, and A. Villringer, "Cross talk in the Lambert-Beer calculation for near-infrared wavelengths estimated by Monte Carlo simulations," *J. Biomed. Opt.* **7**(1), 51–59 (2002).
25. M. Tsuji, A. Duplessis, G. Taylor, R. Crocker, and J. J. Volpe, "Near infrared spectroscopy detects cerebral ischemia during hypotension in piglets," *Pediatr. Res.* **44**, 591–595 (1998).
26. H. Liu, B. Chance, A. H. Hielscher, S. L. Jacques, and F. K. Tittle, "Influence of blood vessels on the measurement of hemoglobin oxygenation as determined by time-resolved reflectance spectroscopy," *Med. Phys.* **22**, 1209–1217 (1995).
27. D. T. Delpy, M. Cope, P. Van Der Zee, S. Arridge, S. Wray, and J. Wyatt, "Estimation of optical pathlength through tissue from direct time of flight measurement," *Phys. Med. Biol.* **33**, 1433–1442 (1988).
28. S. Ijichi, T. Kusaka, K. Isobe, F. Islam, K. Okubo, H. Okada, M. Namba, K. Kawada, T. Imai, and S. Itoh, "Quantification of cerebral hemoglobin as a function of oxygenation using near-infrared time-resolved spectroscopy in a piglet model of hypoxia," *J. Biomed. Opt.* **10**, 024026 (2005).
29. A. Dullenkopf, B. Frey, O. Baenziger, A. Gerber, and W. Weiss, "Measurement of cerebral oxygenation state in anaesthetized children using the INVOS 5100 cerebral oximeter," *Paediatr. Anaesth.* **13**, 384–391 (2003).